# Uncorrelated Interference in 79 GHz FMCW and PMCW Automotive Radar

Overdevest, Jeroen; Jansen, Feike; Laghezza, Francesco ; Uysal, Faruk; Yarovoy, Alexander

**DOI**
10.23919/IRS.2019.8768181

**Publication date**
2019

**Document Version**
Final published version

**Published in**
2019 20th International Radar Symposium (IRS)

**Citation (APA)**
Overdevest, J., Jansen, F., Laghezza, F., Uysal, F., & Yarovoy, A. (2019). Uncorrelated Interference in 79 GHz FMCW and PMCW Automotive Radar. In P. Knott (Ed.), *2019 20th International Radar Symposium (IRS)* (pp. 1-8). Article 8768181 IEEE. https://doi.org/10.23919/IRS.2019.8768181

# Uncorrelated Interference in 79 GHz FMCW and PMCW Automotive Radar

**Jeroen Overdevest***, **Feike Jansen***, **Francesco Laghezza***,
**Faruk Uysal****, **Alexander Yarovoy****

*NXP Semiconductors N.V.
Eindhoven, The Netherlands
email: jeroen.overdevest@nxp.com, feike.jansen@nxp.com, francesco.laghezza@nxp.com

**Delft University of Technology
Delft, The Netherlands
email: f.uysal@tudelft.nl, a.yarovoy@tudelft.nl

***Abstract:*** *An extensive comparison on radar-to-radar interference in frequency-modulated continuous wave (FMCW) and binary phase-modulated continuous wave (PMCW) radars is performed. The noise-plus-interference power for FMCW-to-FMCW and PMCW-to-PMCW interference in a single victim and single interferer environment is compared for generalized waveform-based scenarios. It is proven that the interference suppression is equal in FMCW and PMCW radars in case the time-bandwidth product in both systems is equal.*

## 1 Introduction

Radar sensors have become fundamental instruments in automotive safety applications and advanced driver assistance systems (ADAS). The ADAS applications, such as automatic emergency braking (AEB), adaptive cruise control (ACC), and lane keeping assist (LKA), set high requirements on performance robustness for the safety of human life. To enable new applications, which requires wider coverage, the number of radar sensors per car will increase and data from multiple sensors will be fused. In line with this trend, the number of cars utilizing multiple high-end radar sensors is likely to increase as well (so-called radar penetration rate), which leads to an increased probability of radar-to-radar interference resulting in performance degradation. Interference avoidance techniques, mitigation techniques and a possible radar MAC layer [1] will need to be exploited to counteract the challenges.

Interference in FMCW radars has been a well-established research topic which has been mathematically substantiated by multiple researchers [2, 3, 4, 5]. In contrast, PMCW-to-PMCW interference is a less studied phenomenon. Beise [6] and Bourdoux [7] investigated interference scenarios in FMCW and PMCW automotive radars, but these were mainly case studies, not substantiating the effects of radar-to-radar interference with respect to receiver sensitivity or dynamic range losses. Also, PMCW radars face more challenges in mitigating the noise-like interference, while for FMCW radars mitigation techniques exist, e.g. using time-domain


978-3-7369-9860-5 

notching [4], time-domain reconstruction [8], sparse sampling approaches [9], or (hybrid) digital beamforming techniques [10].
This paper studies multi-user interference and provides a detailed, generalized and non-situation specific, waveform-based study. The paper is organized as follows. Section 2 introduces the basic fundamentals and the measures required to analyze radar-to-radar interference. Sections 3 and 4 provide a detailed investigation substantiated with numerical results on uncorrelated and quasi-correlated interference, respectively. Finally, conclusions are drawn in Section 5.

## 2 FMCW and PMCW Waveform Analysis

In FMCW radar, the transmitters modulate the carrier by linearly increasing the frequency over time for a predefined interval $T_p$, known as a chirp. The FMCW chirp can be defined by its quadratic phase, given as $\phi_M(t) = \pi B/T_p t^2$ with $B$ the radio frequency (RF) chirp bandwidth, which is incorporated in,

$$s_{TX}(t) = \cos\left(2\pi f_c t + \phi_M(t) + \phi_0\right) \mathrm{rect}\left(\frac{t - mT_p/2}{T_p}\right) \tag{1}$$

where $\phi_0$ is any arbitrary initial phase and *rect* denotes the rectangular function. Then, a series of $N_p$ chirps is induced to be able to estimate target velocities. FMCW radars make use of stretch processing, which possesses the desirable characteristic to convert the wideband reflected chirps into narrowband signals. A time-delayed target reflection results in a (narrowband) difference frequency (the so-called beat frequency) between the local oscillator (LO) and the accordingly received echo, which is proportional to the target's range. Phase shifts along the slow-time samples can determine the target's velocity. Using 2D FFT processing, the range and velocity of multiple targets can be efficiently retrieved.

PMCW waveforms are constructed using a code sequence of length $L_c$. The duration of a single coded sequence is equal to $T_p = L_c T_c$ with $T_c$ the duration of a chip. A sequence of $N_p$ codes are transmitted concurrently, having a total measurement time of $T = N_p T_p$. Equation 1 incorporates the bits of the selected sequence with phase shifts $\phi_M(t) \in \{0, \pi\}$ using binary phase-shift keying (BPSK) modulation. The waveform is modulated on a single-carrier frequency $f_c$. After the analog down-conversion, the target's range profile is retrieved by correlating the received signal with the transmitted code, while the target's velocity is estimated in a similar way as in FMCW radar.

FMCW and PMCW are pulse compression waveforms that entail an increase in range resolution and signal-to-noise ratio (SNR). The SNR gain depends on the time-bandwidth product ($BT$) of the modulated waveform [11]. In FMCW radars, the $BT$-product of a single chirp in real Nyquist sampled receivers can be presented in logarithmic form

$$BT_p = 10\log_{10}(B_{IF}T_p) + G_{LPF} = 10\log_{10}\left((F_s/2)\, T_p\right) + G_{LPF} = 10\log_{10}(N_s/2) + G_{LPF}, \tag{2}$$

where $B_{IF}$ represents the intermediate frequency (IF) bandwidth, $N_s$ the number of real-valued ADC samples, and $G_{LPF}$ the gain achieved by low-pass filtering the down-converted signals.

**Table 1:** System Parameters

**(a)** FMCW

| Parameter | Symbol | Value | |
|---|---|---|---|
| Chirp Bandwidth | $B$ | 300 | MHz |
| Chirp Repetition Interval | $T_p$ | 10.64 | µs |
| Sampling rate | $F_s$ | 40 | MHz |
| No. of Samples | $N_s$ | 426 | |
| No. of Chirps | $N_p$ | 1024 | |
| Measurement Time | $T$ | 10.9 | ms |
| Time-Bandwidth Product | $BT$ | 65.15 | dB |

**(b)** PMCW

| Parameter | Symbol | Value | |
|---|---|---|---|
| Code Length | $L_c$ | 3868 | |
| Bit rate | $R_b$ | 300 | MHz |
| Code Repetition Interval | $T_p$ | 12.89 | µs |
| Sampling rate | $F_s$ | 300 | MHz |
| No. of Samples | $N_s$ | 3868 | |
| No. of Code Repetitions | $N_p$ | 845 | |
| Measurement Time | $T$ | 10.9 | ms |
| Time-Bandwidth Product | $R_bT$ | 65.15 | dB |

Stretch processing transforms (desired) target reflections into narrowband baseband signals, while (undesired) noise and interference signals are spread into wideband signals which can be (partly) suppressed by low-pass filtering. Therefore, this gain can be approximated with $G_{LPF} \approx 10\log_{10}(B_{RF}/B_{IF})$ with $B_{IF} = F_s/2$. By coherently adding a series of $N_p$ consecutive chirps, the SNR can be further increased by a factor $N_p$. Thus, the time-bandwidth product of the entire burst of chirps equals $BT_{(dB)} = 10\log_{10}(N_sN_r/2) + G_{LPF}$.

Similarly, the $BT$-product for a single code in PMCW systems equals the code length $BT_p = L_c$. Again, coherent summation of the slow-time periods results in a gain equal to $N_p$. Therefore, the time-bandwidth product of the total code is $BT = L_cN_c$. Table 1a and 1b present the configurations of the reference systems used in this paper. The reference systems are designed to have equal time-bandwidth products for the total measurement duration. In both radars, the transmission parameters are as follows: transmit power $P_T = 10\,\mathrm{dBm}$, the transmit and receive antenna gain $G_T = G_R = 12\,\mathrm{dBi}$, and carrier frequency $f_c = 79\,\mathrm{GHz}$. Let's shortly introduce

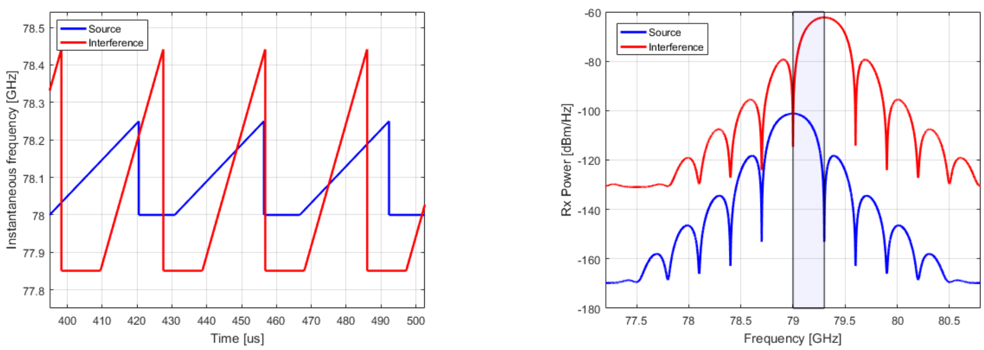


**(a)** Instantaneous frequency in FMCW radars.

**(b)** Time-invariant, sinc-shaped spectrum of single-carrier binary PMCW waveforms.

**Figure 1:** Different time-frequency interference phenomena in FMCW and PMCW radars.

the interference behavior in frequency and time for FMCW and PMCW waveforms. Figure 1a depicts the instantaneous carrier frequency of an FMCW waveform. After the analog mixing stage in the receiver, the difference signal of $K_T$ targets and $K_I$ FMCW interferers can be expressed over time as follows,

$$s_{BB}(t) \propto \sum_{k=1}^{K_T} \exp\left[j2\pi\left(f_{c,S}\tau + \frac{B_S}{T_{p,S}}\tau_k t - \frac{B_S}{2T_{p,S}}\tau_k^2\right)\right] \mathrm{rect}\left(\frac{t - T_{p,S} - \tau_k}{T_{p,S}}\right) +$$

$$\sum_{l=1}^{K_I} \exp\left[j2\pi\left((f_{c,I,l} - f_{c,S})t + f_{c,I,l}\tau_l + \left(\frac{B_{I,l}}{2T_{p,I,l}} - \frac{B_S}{2T_{p,S}}\right)t^2 - \frac{B_{I,l}}{2T_{p,I,l}}(2t\tau_l + \tau_l^2)\right)\right] \mathrm{rect}\left(\frac{t - T_{p,I,l} - \tau_l}{T_{p,I,l}}\right) \quad (3)$$

where $\tau$ denotes the victim-to-interferer time delay, the parameter subscripts $S$ and $I$ denote the source and interferer, respectively. Equation 3 shows that the interference signal after mixing still is in the form of a frequency ramp due to its quadratic phase.
Figure 1b shows the frequency spectrum of a PMCW waveform. Due to the rectangular-shaped chips used in the coded waveform, the spectrum of an PMCW waveform has a sinc-shape. The spectrum is non-interrupted, time-invariant due to a $100\%$ duty cycle to leverage the more enhanced periodic correlation properties. This means that the interference energy will be present for consecutive ADC samples in the source, while FMCW-to-FMCW interference has a discontinuous interference presence as a result of the low-pass filtered de-ramped signal.

This paper considers uncorrelated interference, meaning that the source and interferer waveform do not share the *exact* same time-instantaneous resources: carrier frequency $f_c$, bandwidth $B$, and code properties (family, code itself, and length). A very specific case with distinctive overlap in time of the victim and interference waveforms, which we will refer to as quasi-correlated interference, results in a different interference behavior that will be addressed in Section 4.

## 3 Uncorrelated Radar-to-Radar Interference

Radar-to-radar interference might occur when two radars with common field of view transmit an arbitrary waveform, illuminating each other by line-of-sight (LOS) or non-line-of-sight (NLOS), and sharing time and frequency resources, which can be defined in ratios as $\gamma_T = T_I/T_S$ and $\gamma_B = B_{OL}/B_S$, respectively. Here, two source and interfering signal vectors, $s_{RX,S}(t)$ and $s_{RX,I}(t)$, share the same bandwidth $B_{OL} = (B_S + B_I)/2 + |f_{c,I} - f_{c,S}|$. Now, a generalized non-waveform based interference scenario can be defined using the triplet $(\gamma_T, \gamma_B, P_{R,I})$, with $P_{R,I}$ being the received interference power at the victim antenna.

For numerical analysis, we have sketched the following scenario: three static targets at distances $R_T = 5, 30, 60\,\mathrm{m}$ all having a radar cross section (RCS) of $0\,\mathrm{dBsm}$, and a single interferer at $R_I = 10\,\mathrm{m}$. Figure 2a shows the Range-Doppler map in the absense of interference where all targets can be detected. The (desired) target reflected signals experience the coherent processing gain according to the RF time-bandwidth product relative to the noise power, thus resulting in a signal-to-noise ratio (SNR) gain. In this case, the noise floor is equal to the thermal noise power, which depends on the receiver bandwidth $B_{IF}$, and is $P_{N_{(dB)}} = -174 + F_N = -159\,\mathrm{dBm/Hz}$ given the receiver noise figure $F_N = 15\,\mathrm{dB}$.
With the victim configuration according to Table 1, results of having an active interferer illuminating the victim are shown in Figure 2b-2f for a received interference power $P_{R,I_{(dB)}} = -56.40\,\mathrm{dBm}$ at the victim's receive antenna, where the signal covers the complete

victim's RF bandwidth $\gamma_B = 100\%$ and has a time presence of $\gamma_T = 100\%$. Figure 2b presents a FMCW-to-FMCW interference scenario where the interfering chirp is completely randomized and incoherent in time during the acquisition period $T_{p,S}$. Then, the interference energy spreads out uniformly. However, in practice the frequency chirp and time (PRI) for both the source and interferer do not change during the measurement time $T_S$ (as depicted in Figure 1a). In this scenario, the noise floor is not completely flat, showing specific (diagonal) patterns, due to the residual coherence over the slow-time samples, after Doppler processing. By observing Figure 2d-2f, PMCW interference can be classified as highly uncorrelated leading to an uniform increase in noise floor. The interference samples appear as noise, therefore, the victim's correlation output is undeterministic. Hence, no apparent pattern along the slow-time periods is observable after range and Doppler processing. Therefore, the consecutive slow-time outputs of range processing are incoherently added in the Doppler FFT, leading to the noise-like behavior.

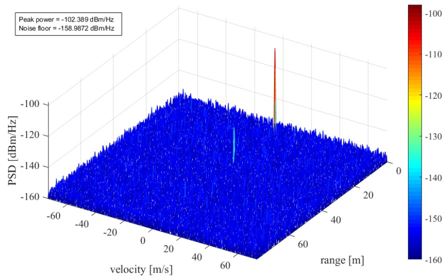


**(a)**

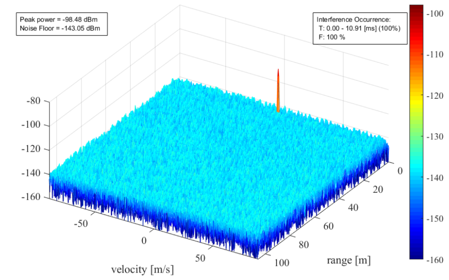


**(b)**

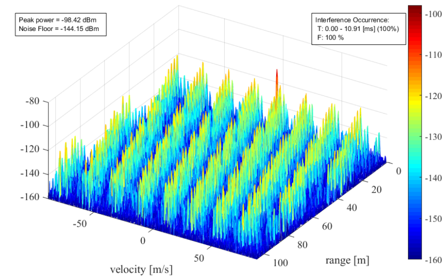


**(c)**

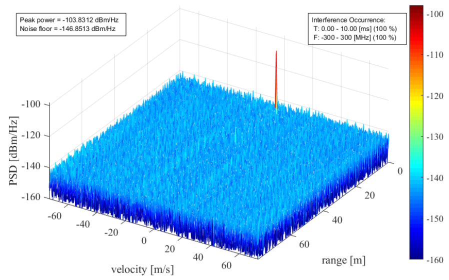


**(d)**

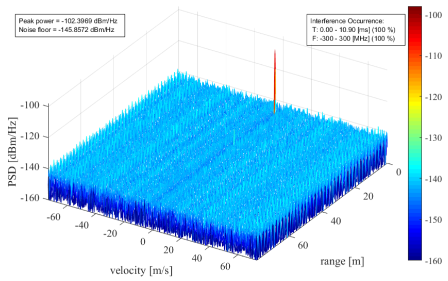


**(e)**

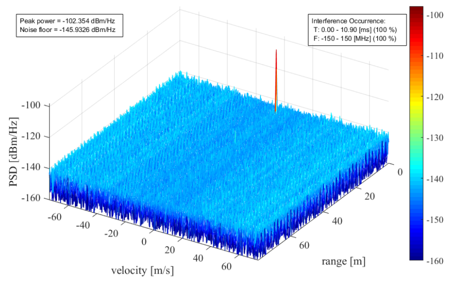


**(f)**

**Figure 2:** Non-interfered scenario in (a) and uncorrelated interference scenarios for (b-c) FMCW-to-FMCW and (d-f) PMCW-to-PMCW with different interference configurations: (d) different code families [APAS(3868), ZCZ(4096)], (e) different code length [APAS(3868), APAS(3864)], and (f) different bit rates [APAS(3868), APAS(1308)].

Using the link budget model, the noise-plus-interference power can be theoretically expressed as,

$$IN = 10\log_{10}\left(P_N + P_{R,I_{10m}}\right) - 10\log_{10}(B_{IF}) = -141.1\,\mathrm{dBm/Hz}\ . \tag{4}$$

Comparing (4) to the results of uncorrelated interference from Figure 2, shows that the noise floors in the Range-Doppler Maps measured in power spectral densities yield in $(2b)$ $-143.05\,\mathrm{dBm/Hz}$, $(2c)$ $-144.15\,\mathrm{dBm/Hz}$, $(2d)$ $-146.91\,\mathrm{dBm/Hz}$, $(2e)$ $-145.86\,\mathrm{dBm/Hz}$, and $(2f)$ $-145.93\,\mathrm{dBm/Hz}$. The decrease in dynamic range due to interference presence causes the targets at $R_T = 30$ and $60\,\mathrm{m}$ to fall below the noise floor. The measured values are slightly lower compared to the value calculated in (4). In addition to the average noise floor increase given the interference time occurrence $\gamma_T$ as defined in [12], the interference power present after processing also depends on the time interval taking into account the FFT window suppression,

$$P_{I,_{post-proc}} = P_{R,I(dBm)} - 10\log_{10}\left(\gamma_T\right) - L_{win}\ , \tag{5}$$

where $L_{win}$ defines the suppression gain from the applied window.

To further explore the interference energy levels in FMCW and PMCW radars, a series of Monte Carlo simulations have been executed considering randomized interference occurrences and configurations. The randomized parameters include $f_c$, $B$, $T_p$, as well as the code selected from its family for PMCW interference. Figure 3 shows the comparison among the simulated noise floors Range-Doppler outputs for the FMCW and PMCW reference systems in the presence of increasing received interference power levels. Respectively, Figures 3a-3c depict the noise floor outputs for the time-occurrences $\gamma_T = 5\%$, $25\%$, and $70\%$, which can be individually compared using (5). Small differences in the post-processing noise floor between the FMCW and PMCW reference systems can be explained by disparities in the architectural designs.

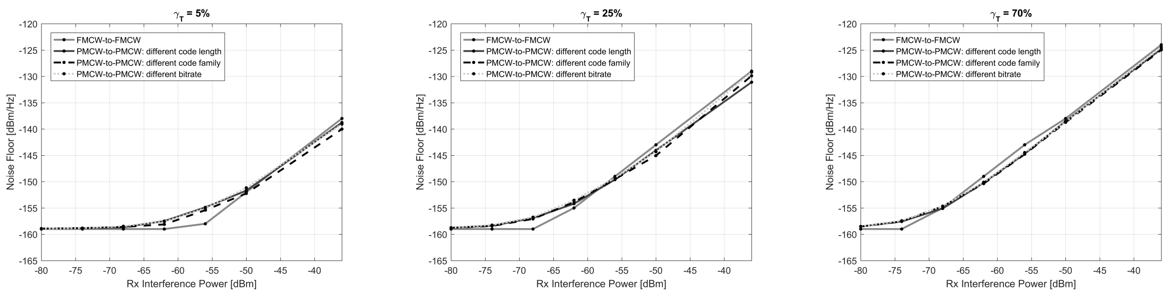


(a) (b) (c)

**Figure 3:** Measured noise floor levels [in $\mathrm{dBm/Hz}$] for different interference occurrences in time: (a) $\gamma_T = 5\%$, (b) $\gamma_T = 25\%$, and (c) $\gamma_T = 70\%$.

## 4 Quasi-correlated Radar-to-Radar Interference

In contrast to uncorrelated interference, situations can arise where radar-to-radar interference results in a non-uniform increase of the noise floor after post-processing. Regardless of the frequency or coding resources, this occurs when the pulse repetition interval (PRI) of the victim

and interferer is in the form of $T_{p,S} = nT_{p,I}$ with $n$ being an integer or its reciprocal.
For example, when $n = 2$, every slow-time period of the victim fits in precisely two periods of the interferer. This means that the phase-relation over the slow-time samples remains constant, and the interference energy is concentrated in a single dimension in the zero-Doppler cut. In case the interferer is moving, or radiating at a deviating carrier frequency, the ridge is moving to the corresponding offset Doppler frequency. As the offset in carrier frequency exceeds the victim's maximum unambiguous velocity, the ridge aliases to the negative frequencies due to back-folding. This phenomenon of spectrum folding withholds the system from estimating the corresponding frequency offset, because of ambiguity.

The effects of quasi-correlated interference have been presented in Figure 4, for $n = 2$, for FMCW and PMCW, respectively, in which a distance ridge is concentrated in the zero-Doppler gate, since both victim and interferer are transmitting at similar carrier frequency $f_c$ and are moving at zero relative radial speed. For FMCW-to-FMCW, the RF chirp bandwidth was equal for both cases $B_S = B_I = 300\,\text{MHz}$ with the victim's chirp time $T_{chirp,S} = 12.8\,\mu\text{s}$ and reset time $T_{reset,S} = 10.3\,\mu\text{s}$, and the interferer's chirp time $T_{chirp,I} = 8.09\,\mu\text{s}$ and reset time $T_{reset,I} = 3.46\,\mu\text{s}$. Hence, both victim's and interferer's period duration $T_p = T_{chirp} + T_{reset}$ satisfy $T_{p,S} = 2T_{p,I}$. Similarly, the quasi-correlated interference situation for PMCW was configured with both victim and interferer transmitting at a similar bitrate $R_b$, but using code lengths of $L_{c,S} = 4096$ and $L_{c,I} = 2048$, respectively.

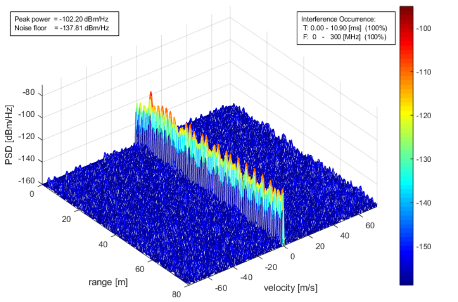


**(a)** FMCW-to-FMCW

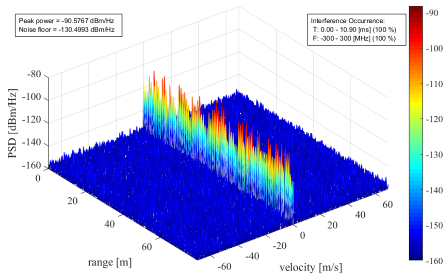


**(b)** PMCW-to-PMCW

**Figure 4:** Quasi-correlated interference with equivalent PRIs: $T_S = 2T_I$

## 5 Conclusion

In this paper, we have investigated and compared the impacts of uncorrelated and quasi-correlated interference on FMCW and PMCW radar systems. Regardless of the waveform being used, the interference energy after range and velocity processing is equal, and it behaves according to the RF time-bandwidth product. Both radar systems have to account for similar losses in the receiver sensitivity assuming an equal received interference power.
For FMCW, uncorrelated interference leads to a diagonal ridges in the range-Doppler spectrum that depends on the ratio between the slopes of the victim and interferer. In PMCW radars, the interference energy is uniformly spread out over the whole Range-Doppler map.
Also, we have presented under which conditions (equal or multiple PRIs) a form of quasi-correlated interference can arise for both reference systems.

## 6 Future Work

The conclusion that FMCW and PMCW pulse-compressed waveforms experience equivalent interference-driven noise floors, according to the RF time-bandwidth product, does not indicate that the chance on interference for both radar systems is equal when taking into account waveform and system architecture aspects. Therefore, before being able to claim which waveform can better reject interference, the probability of interference occurrence in FMCW and PMCW radars needs to be identified, including a study on the probability of uncorrelated and correlated interference.

## 7 Acknowledgments

This paper has emerged from the first author's Master Thesis from Delft University of Technology, which was done in cooperation with NXP Semiconductors. The first author wants to show his gratitude to both organizations for the provided facilities, supervision, and assistance.

## References

[1] J. Khoury, R. Ramanathan, D. McCloskey, R. Smith, and T. Campbell, "Radarmac: Mitigating radar interference in self-driving cars," in *2016 13th Annual IEEE International Conference on Sensing, Communication, and Networking (SECON)*, pp. 1–9, June 2016.

[2] G. M. Brooker, "Mutual interference of millimeter-wave radar systems," *IEEE Transactions on Electromagnetic Compatibility*, vol. 49, pp. 170–181, Feb 2007.

[3] M. Goppelt, H. . Blcher, and W. Menzel, "Analytical investigation of mutual interference between automotive fmcw radar sensors," in *2011 German Microwave Conference*, pp. 1–4, March 2011.

[4] J. Bechter, K. D. Biswas, and C. Waldschmidt, "Estimation and cancellation of interferences in automotive radar signals," in *2017 18th International Radar Symposium (IRS)*, pp. 1–10, June 2017.

[5] M. Goppelt, H.-L. Blöcher, and W. Menzel, "Automotive radar - investigation of mutual interference mechanisms," *Advances in Radio Science*, vol. 8, pp. 55–60, 2010.

[6] H. Beise, T. Stifter, and U. Schrder, "Virtual interference study for fmcw and pmcw radar," in *2018 11th German Microwave Conference (GeMiC)*, pp. 351–354, March 2018.

[7] A. Bourdoux, K. Parashar, and M. Bauduin, "Phenomenology of mutual interference of fmcw and pmcw automotive radars," in *2017 IEEE Radar Conference (RadarConf)*, pp. 1709–1714, May 2017.

[8] F. Uysal and S. Sanka, "Mitigation of automotive radar interference," in *2018 IEEE Radar Conference (RadarConf18)*, pp. 0405–0410, April 2018.

[9] F. Uysal, "Synchronous and asynchronous radar interference mitigation," *IEEE Access*, pp. 1–1, 2018.

[10] J. Bechter, K. Eid, F. Roos, and C. Waldschmidt, "Digital beamforming to mitigate automotive radar interference," in *2016 IEEE MTT-S International Conference on Microwaves for Intelligent Mobility (ICMIM)*, pp. 1–4, May 2016.

[11] M. Jankiraman, N. Willis, and H. Griffiths, *Design of Multi-Frequency CW Radars*. Electromagnetics and Radar, Institution of Engineering and Technology, 2007.

[12] S. Murali, K. Subburaj, B. Ginsburg, and K. Ramasubramanian, "Interference detection in fmcw radar using a complex baseband oversampled receiver," in *2018 IEEE Radar Conference (RadarConf18)*, pp. 1567–1572, April 2018.